Research on Chemical Intermediates
https://doi.org/10.1007/s11164-020-04100-3

Facile one-pot synthesis, butyrylcholinesterase and α-glucosidase inhibitory activities, structure–activity relationship, molecular docking and DNA–drug binding analysis of Meldrum's acid derivatives

Haroon Mehfooz, et al. ***[full author details at the end of the article]***

Received: 18 July 2019 / Accepted: 7 February 2020

Abstract

Meldrum's acid derivatives were facile synthesized by one-pot condensation process and characterized by NMR (^{1}H, ^{13}C, DEPT-90 and DEPT-135) and EI-MS. The synthesized compounds were screened for their potential to inhibit butyrylcholinesterase (BChE) and α-glucosidase enzymes. Interestingly, the derivative **3a** showed potent α-glucosidase inhibitory activity, with the IC_{50} value equal to 2.1 mg/mL as compared to standard acarbose (IC_{50} = 4.7 mg/mL), whereas, in terms of BChE inhibitory activity investigation, the derivatives **3a** and **3c** showed novel results, with the IC_{50} values equal to 1.2 and 2.9 mg/mL, respectively, as compared to standard galantamine hydrobromide (IC_{50} = 4.7 mg/mL), making derivative **3a** a dual inhibitor of both enzymes. Further, structure–activity relationship, comparative molecular docking analysis and the DNA–drug binding interaction were studied to investigate relationship between the chemical structure and its biological activity, inhibition of mechanism, interaction of compounds, DNA binding constant and Gibbs free energy. Structural insights into inhibitor binding to the α-glucosidase and BuChE revealed significant contribution of hydrophobic regions and significant residues of active sites. Comparative molecular docking studies showed that the residues of oxyanion hole, catalytic triad and hydrophobic pocket were actively engaged in interaction with the inhibitor. DNA binding constant was found in the order K_b 3e > K_b 3c > K_b 3a > K_b 3b > K_b 3d, while Gibbs free energy was found in the order ΔG 3e > ΔG 3a > ΔG 3b > ΔG 3c > ΔG 3d.

Keywords Meldrum's acid · α-Glucosidase · Butyrylcholinesterase · Molecular docking · DNA–drug interaction · DFT calculations

Introduction

Alzheimer's disease (AD), a type of dementia, is a progressive neurodegenerative disorder commonly occurring in the elderly people above 40s. The most common form of dementia is dementia with Lewy bodies (DLB) and is characterized by loss

of memory, behavior and other cognitive deficiencies. Pathologically, AD is characterized by loss of cholinergic neurons, deposition of plaque and neurofibrillary tangles (NFTs) within the central nervous system. This deposition of plaque and neurofibrillary tangles takes place within the cortex and hippocampus, areas of the brain associated with higher cognitive functions and memory [1, 2]. These plaques are mainly consisted of amyloid β-peptide (Aβ42), and interestingly, cholinergic synaptic function is considered to be particularly susceptible to β-amyloid peptide toxicity. Thus, the loss of synaptic vesicles on axon terminals may cause cholinergic neuronal loss [3, 4]. In order to treat AD, various drugs have been disclosed in the literature such as multi-targetable chalcone analogs [5], amino acids/peptides conjugated heterocycles [6], chloro-containing molecules [7], sulfur (SVI)-containing motifs [8], benzisoxazole [9], tetralone derivatives [10], α,β-unsaturated carbonyl-based cyclohexanone derivatives [11], tetramethylpyrazine-based chalcone derivatives [12], podophyllotoxin derivatives [13] and ligustrazine-based cyclohexanone and oxime analogs [14].

Butyrylcholinesterase (BChE, EC 3.1.1.8) belongs to the family of enzymes known as cholinesterase. It plays an important role in the hydrolysis of acetylcholine (ACH), a neurotransmitter in the brain, which results in the termination of impulse transmission at cholinergic synapses [15]. As discussed earlier, Alzheimer's disease is characterized by the loss of cholinergic neurons, resulting in decreased levels of BChE; this lack of butyrylcholine manifests itself in different symptoms such as loss of memory, impaired intellectual abilities and cognitive dysfunction [16]. Thus, cholinesterase is an important target in the treatment of AD and various cholinesterase inhibitors (ChEI) have been developed, i.e., donepezil, rivastigmine and tacrine, and they act by increasing the availability of ACh in central synapses [17].

Diabetes mellitus continues to be a serious threat to human health. Medicinal chemists have devoted their efforts to uncover the complications associated with lethal disease, diabetes [18, 19]. It is believed that advanced glycation end products (AGEs) mediate several diabetic complications. Glycation of non-enzymatic lipids or proteins produces the AGEs via condensation, fragmentation and oxidative modifications by reducing sugars. The rise in these AGEs significantly increases the chances of diabetes and other cardiovascular diseases. Thus, inhibition of protein glycation can be an effective approach to minimize complications of diabetes. Currently available medication for treatments of diabetes is insulin and various oral antidiabetic agents, such as biguanides, sulfonylureas and glucosidase inhibitors, but most of these accessible antidiabetic agents have few serious adverse effects [20–24]. To fully cope with the diabetes, the development of efficient and risk-free diabetic agents is the need of the hour.

Meldrum's acid derivatives are remarkable organic synthon (Fig. 1) and are widely employed in the synthesis of natural products and heterocyclic cores [25, 26]. Besides being versatile synthon, Meldrum's acid derivatives exhibit encompassing spectrum of biological activities. They show antibacterial, antimicrobial, antimalarial, antioxidant and HIV-1 inhibitor activities [27, 28]. The well-recognized synthetic and biological significance of Meldrum's acid prompted us to synthesize C-5-substituted novel derivatives by condensation reaction of different substituted anilines with Meldrum's acid.

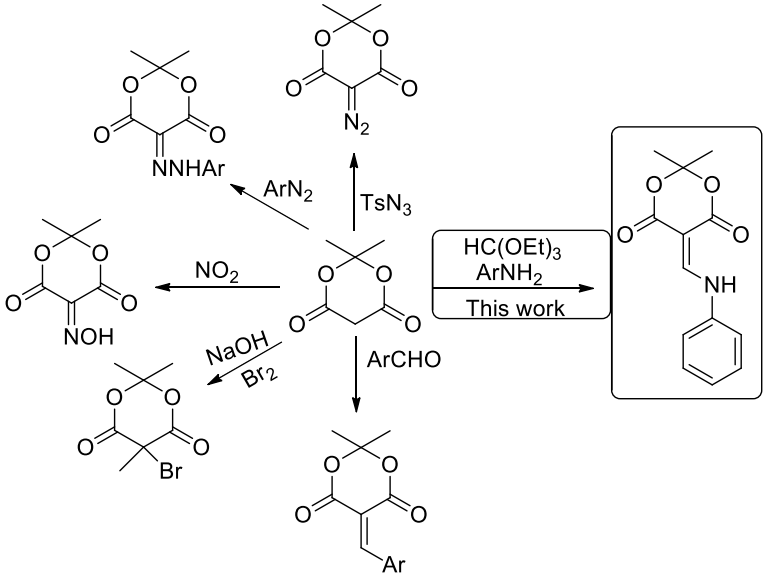

Fig. 1 Synthetic utility of Meldrum's acid in organic synthesis

Due to excellent activities, in this research work, we have synthesized Meldrum's acid derivatives by one-pot simple condensation process and characterized these derivatives by NMR and EI-MS. The synthesized compounds were screened for their potential to inhibit butyrylcholinesterase (BChE) and α-glucosidase enzymes. Structure–activity relationship, comparative molecular docking analysis, the DNA–drug binding interaction and computational investigations have also been done.

Experimental

Methods and materials

All the reagents and chemicals were purchased commercially and were further purified prior to use. Thin-layer chromatography was performed using silica gel-coated aluminum sheets (Merck). Melting point was taken three times using a Gallenkamp apparatus. Mass spectra were recorded with JEOL MS route operated with electron ionization mode with Varian MAT312. ^{1}H NMR spectra were recorded in d6-DMSO with Bruker AM 300 and AM 400 spectrometers (Rheinstetten-Forchheim, Germany) operating at 300 MHz and 400 MHz, respectively. ^{13}C NMR spectra were recorded in DMSO-d6 with Bruker AM 300 spectrometer (Rheinstetten-Forchheim, Germany) operating at 75.5 MHz, respectively. Tetramethylsilane was taken as an internal standard in NMR spectra.

General procedure for synthesis of (3a–3e)

In a 50-mL round-bottom flask, Meldrum's acid (0.3 g, 0.002 mol) and equimolar respective amino compounds were allowed to react in the presence of slightly excess triethyl orthoformate (0.98 g, 0.06 mol) in 2-butanol (5 mL) as a solvent. The reaction mixture was refluxed for 3–5 h. The solid formed in hot state was collected by suction filtration. Washing with ethanol furnished TLC pure compound in excellent yield. The purity of the synthesized compounds was checked by thin-layer chromatography using ethyl acetate and n-hexane (2:8), dichloromethane and n-hexane (4:6) and ethyl acetate and methanol (1:9) composition solvent systems.

Experimental data

2,2-Dimethyl-5-{[3-(trifluoromethylphenyl]amino}methylene)-1,3-dioxane-4,6-dione (3a)

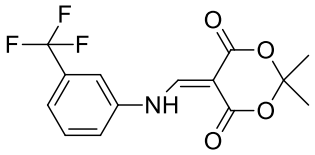

Yield: 80%, yellow, m.p. 148 °C. ^{1}H NMR (300 MHz, DMSO-d_6 δ:11.3 (1H, s, CH–NH), 8.6 (1H, s, CH–NH), 8.1 (1H, s, ArH), 7.9 (1H, d, *J* 8, ArH), 7.5–7.6 (2H, m, ArH), 1.6 (6H, s, 2xCH_3); ^{13}C NMR (75.5 MHz, DMSO-d_6) δ: 163.5, 162.6, 153.8, 139.5, 130.5, 129.5, 125.1, 123.1, 122.4, 122.3, 104.1, 87.5, 26.4; EI-MS (EI): *m*/*z* 314.8 (M+ 23.4%), 257.8 (39.2), 256.7(64.5), 211.9 (100), 184.9 (65.8), 115.9 (14.9), 52.9 (62.9). Anal Calc: $C_{14}H_{12}F_3NO_4$; C, 53.34, H, 3.85, N, 4.65. Found, C, 54.37, H, 4.53, N, 5.04.

4-{[(2,2-Dimethyl-4,6-dioxo-1,3-dioxan-5-ylidene)methyl]amino}-2-hydroxybenzoic acid (3b)

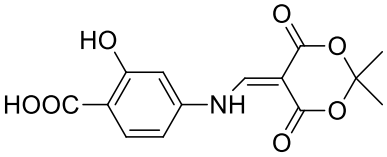

Yield: 77%, brown, m.p. 192 °C. ^{1}H NMR (300 MHz, DMSO-d_6) δ:11.1 (1H, d, CH–NH), 10.8 (1H, s, COOH), 8.5 (1H, d, CH–NH), 7.2 (1H, t, J 8, ArH), 6.9 (1H, d, ArH), 6.8 (1H, s, ArH), 6.6 (1H, m, OH), 1.7 (6H, s, 2xCH_3); ^{13}CNMR (75.5 MHz, DMSO-d_6) δ: 163.8 (C), 162.7 (C), 158.3 (C), 152.8 (CH), 139.5 (C)

131.7 (C), 113.4 (CH),109.4 (CH), 105.7 (CH), 105 (C), 104.1 (C), 86.4 (C), 26.4 (CH_3); MS (EI): *m/z* 262.8 (M+ 18.5%), 204.9 (48.3), 159.9 (68.3), 132.9 (100), 104.9 (38.4), 65.0 (34.5). Anal Calc: $C_{14}H_{13}NO_7$; C, 54.84, H, 4.35, N, 5.65. Found, C, 55.37, H, 5.53, N, 5.04.

2,2-Dimethyl-5-({[2-(trifluoromethyl)phenyl]amino} methylidene)-1,3-dioxane-4,6-dione (3c)

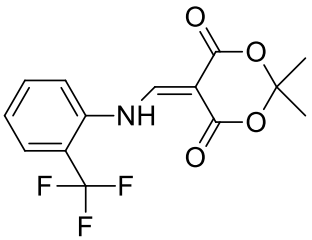

Yield: 73%, dark yellow, m.p. 120 °C. ^{1}H NMR (300 MHz, DMSO-d_6) δ: 11.6 (1H, d, *J* 12.8, CH–NH), 8.7 (1H, d, *J* 12.8, CH–NH), 7.9 (1H, d, *J* 8, ArH),7.4 (1H, m, J 7.7, ArH), 7.7 (1H, m, ArH), 1.7 (6H, s, $2CH_3$); ^{13}C NMR (300 MHz, DMSO-d_6) δ: 164.3 (C), 162.0 (C), 154.8 (CH), 135.8 (C) 134.4 (CH), 126.7(CH),126.6 (CH), 126.6 (C), 120.8 (CH), 118.6 (C), 104.1 (C), 88.5 (C), 26.4 (CH_3); MS (EI): *m/z* 314.7 (M+ 7.7%), 256.7 (65.6), 211.9 (48.8), 191.9 (22.6), 113.8 (10.9), 82.9 (100), 53 (37.3). Anal Calc: $C_{14}H_{12}F_3NO_4$; C, 53.34, H, 3.85, N, 4.65. Found, C, 54.37, H, 4.53, N, 5.04.

2,2-Dimethyl-5-{[(2-methyl-3-nitrophenyl)amino]methylid} ene)-1,3-dioxane-4,6-dione (3d)

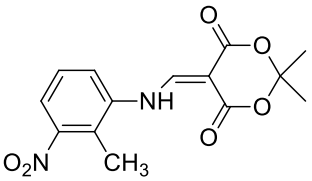

Yield: 83%, light yellow, m.p. 160 °C. ^{1}H NMR (300 MHz, DMSO-d_6) δ: 11.3 (1H, d, J 13.8, CH–NH), 8.5 (1H, d, *J* 14.1, CH–NH), 7.9 (1H, d, *J* 7.8, ArH), 7.7 (1H, m, J 7.8, ArH), 7.5 (1H, m, J 8.1, ArH), 2.4 (3H, s, CH_3), 1.7 (6H, s, $2CH_3$); ^{13}C NMR (300 MHz, DMSO-d_6) δ: 164.5 (C), 162.4 (C), 155.5 (CH), 150.8 (C), 139.3 (C) 127.9 (CH), 123.8 (CH),123.6 (C), 121.6 (CH), 104.4 (C), 87.5 (C), 26.4 (CH_3), 12.9 (CH_3); MS (EI): *m/z* 305.8 (M+ 10.6%), 247.8 (83.7), 188.9 (47.9), 158.9 (19.9), 76.9 (100). Anal Calc: $C_{14}H_{14}N_2O_6$; C, 54.91, H, 4.65, N, 9.15. Found, C, 55.37, H, 5.53, N, 10.04.

5-{[(3-Fluorophenyl)amino]methylidene)-2,2-dimethyl-1,3-dioxane-4,6-dione (3e)

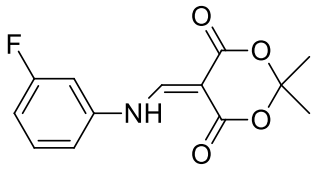

Yield: 79%, light yellow, m.p. 144 °C. ^{1}H NMR (300 MHz, DMSO-d_6) δ: 11.2 (1H, s, CH–NH), 8.5 (1H, s, CH–NH), 7.5 (1H, m, ArH), 7.4-7.5 (2H, m, ArH), 7.0-7.1 (1H, m, ArH), 1.7 (6H, s, 2CH_3); ^{13}C NMR (300 MHz, DMSO-d_6) δ:164.2 (C), 160.9 (C), 153.4 (CH), 140.5 (C), 140.3 (C), 131.3 (CH), 115.1 (CH), 112.9 (CH), 106.7 (CH), 104.2 (C), 86.4 (C), 26.4 (2CH_3); MS (EI): *m/z* 265 (M+ 16.3%), 249.9, 207 (64.2), 162 (92.8), 135 (100), 53 (56.4). Anal Calc: $C_{13}H_{12}FNO_4$; C, 58.88, H, 4.57, N, 5.35. Found, C, 59.37, H, 5.53, N, 6.04.

Methods of bioassay

α-Glucosidase assay

α-Glucosidase enzyme inhibition assay was performed according to the previously reported method [20]. For experiment, 25 µL *p*-nitrophenyl–α-D-glucopyranoside, 65 µL phosphate buffer (pH 6.8) and 5 µL α-glucosidase enzyme (0.05 U/mL) were mixed in a 96-well microtiter plate. Five microliters compound with the final concentrations of 500, 250 and 125 µg/mL was added in respective wells. Acarbose and DMSO were used as positive and negative controls, respectively. Plates were incubated at 37 °C for 30 min, followed by the addition of 0.5 mM sodium bicarbonate (100 µL) as a stopping agent. Absorbance was measured at 405 nm using a microplate reader (BioTek Elx-800, USA), and IC_{50} was calculated by using GraphPad Prism 5.

Butyrylcholinesterase assay

Ellman's method was used to determine the butyrylcholinesterase enzyme inhibition potential of the compound [21, 22]. The compound (5 µL) with the final concentrations of 500, 250 and 125 µg/mL was mixed with 20 µL of 100 µM phosphate buffer (pH 8.0) and 5 µL BChE enzyme (0.05 U/mL). Then, 10 µL butyrylthiocholine iodide (4 mM) and 60 µL DTNB (3 mM) were added. Galantamine hydrobromide and DMSO served as positive and negative controls, respectively. The reaction mixtures were then incubated for 30 min at 37 °C. After incubation, absorbance was measured at 405 nm using a microplate reader (BioTek Elx-800, USA) and IC_{50} was calculated by using GraphPad Prism 5.

Methodology for molecular docking

The crystal structures of α-glucosidase and butyrylcholinesterase (PDB IDs: 4LBS and 1A27) were retrieved through PDB (http://www.rcsb.org). 2D structures of compounds were generated by ChemDraw (http://www.cambridgesoft.com) tool, followed by geometrical optimization with LigandScout [23]. Each compound was virtually docked against α-glucosidase and butyrylcholinesterase (BuChE) through AutoDock 4.2 [24] suit of PyRx to achieve an optimal complementarity of steric and physiochemical properties. The number of runs for each docking was set to 100. The Lamarckian genetic algorithm (LGA) was applied to the following parameters: initial population of 150 randomly placed individuals, a maximum number of 27,000 generations, a mutation rate of 0.02, 2.5×10^6 energy evaluations and a crossover rate of 0.80, while the remaining docking parameters were set to default. For the purpose of attaining the best binding pose, these inhibitors were comparatively docked through PatchDock [25]. Afterward, hydrophobic and electrostatic interactions were mapped using LigPlus [26] and visualized by UCSF Chimera 1.9.0 [27].

Results and discussion

Chemistry

Synthesis

Compounds (**3a**–**3e**) were obtained in good yield ranging from 73 to 83%, by treating different aromatic amino compounds with Meldrum's acid in the presence of triethyl orthoformate using 2-butanol as shown in Scheme 1 [29–31].

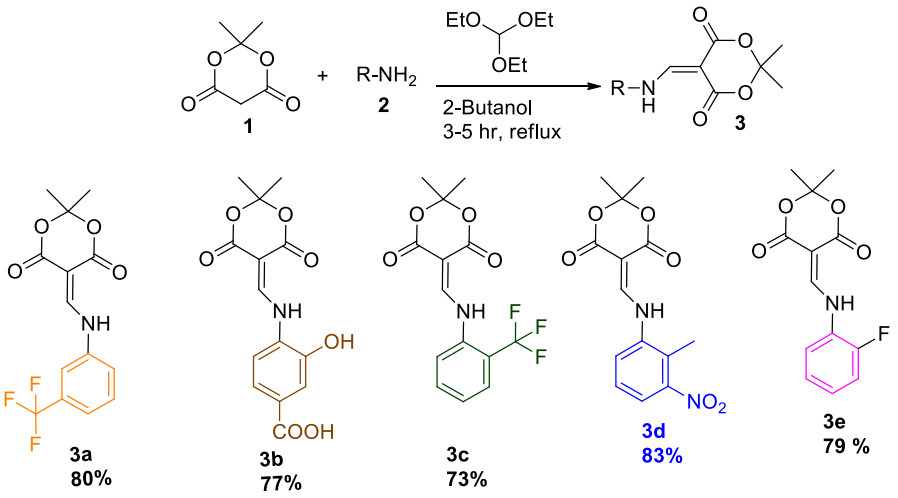

Scheme 1 Synthetic route toward the synthesis of novel Meldrum's acid derivatives (**3a**–**3e**)

Spectroscopic characterization

Structures of all these compounds were elucidated by spectroscopic technique NMR (^{1}H, ^{13}C, DEPT-90 and 135) and mass spectrometry. ^{1}H NMR spectra of compounds showed that (=CH–NH) proton appeared as doublet at δ 11.1–11.6. Similarly, (=CH–NH) proton of compounds also displayed doublet at δ 8.4–8.7. Both have same *J* value, which proves that these are coupling partners. An intense singlet displayed at δ 1.6–1.7 of six protons integral for two methyl groups attached at C2. The ^{13}C NMR spectra of compounds (**3a**–**3e**) showed that both cyclic quaternary carbonyl carbons (C-2 and C-6) in all compounds appeared at δ 151.9–162.7 and δ 152.8–164.9, respectively. In all the compounds, methylidene carbon displayed signal at δ 152.8–155.5. DEPT-90 proved it and appeared downfield due to the direct attachment of methylidene carbon with inductively electron-withdrawing nitrogen atom and also due to conjugation with carbonyl group. Similarly, C-2 quaternary carbon displayed signal at δ 104.1–174.7, while C-5 quaternary carbon showed singlet at δ 86.1–88.5. The two methyl groups exhibited signal at δ 26.4–26.4. DEPT-135 confirmed the presence of methyl groups and CH groups by the appearance of positive signals.

The mass spectrometry analysis also provided evidence of formation of products. The two methyl groups of Meldrum's acid were confirmed by the loss of acetone by Retro–Diels–Alder fragmentation pattern, resulting in the cyclic lactone having $m/z = 207$. The loss of CO from cyclic lactone resulted in the formation of acyclic carboxylic acid having a triple bond (Scheme 2).

Biological activity

α-Glucosidase assay

The antidiabetic potential of the compounds was evaluated by using commercial purified α-glucosidase enzyme. The assay was performed in triplicate, and results are presented in Table 1. Acarbose was used as a positive control, and DMSO served as a negative control. The results showed that **3a** compound showed α-glucosidase inhibitory activity with the IC_{50} value of 2.1 mg/mL which is higher than the standard acarbose ($IC_{50} = 4.7$ mg/mL). The other four derivatives were also found as potent derivatives.

Butyrylcholinesterase assays

The synthesized compounds were tested for their activity against butyrylcholinesterase enzyme. The assay was performed in triplicate, and results are shown in Table 2. Galantamine hydrobromide was used as a positive control. The results showed that the highest activity was exhibited by compounds **3a** and **3c** (IC_{50} values 1.2 and

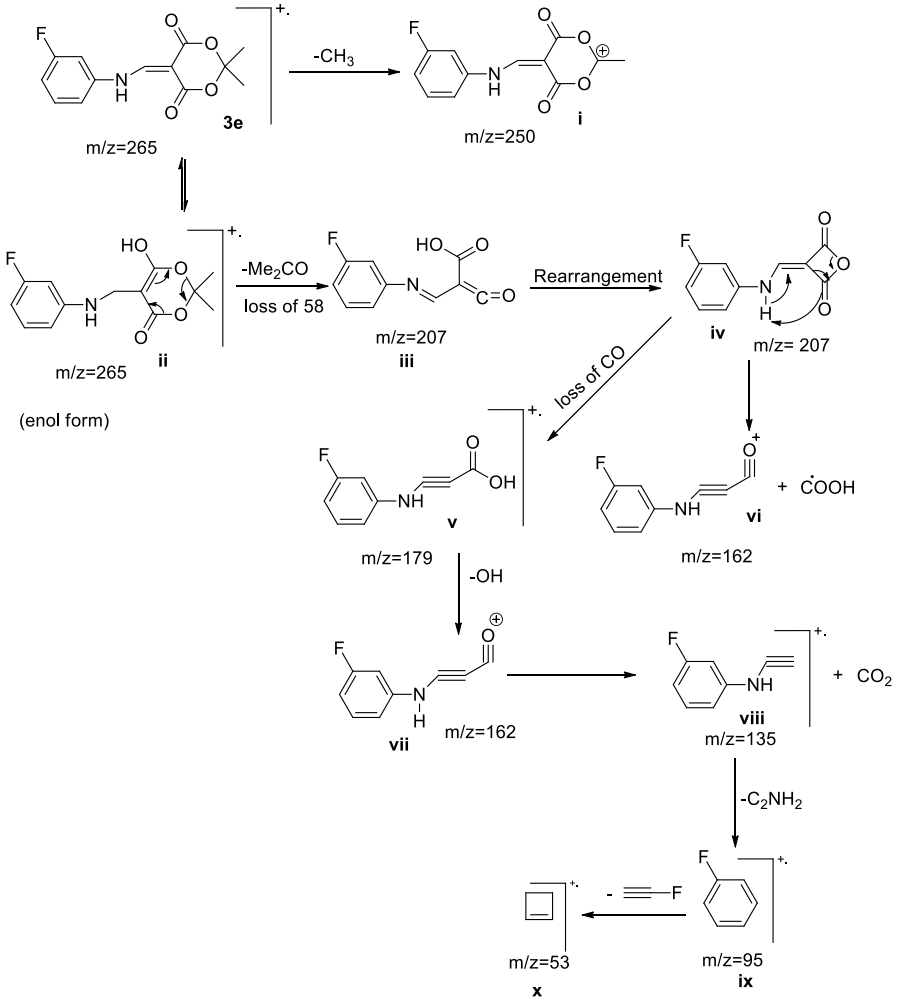

Scheme 2 EI-MS fragmentation of compound **3e**

Table 1 Results of α-glucosidase activities analysis (IC_{50} values of Meldrum's acid derivatives (**3a**–**3e**) using acarbose as standard)

S. no.	Compound codes	IC_{50} (mg/mL)
1	**3a**	2.1
2	**3b**	12
3	**3c**	10
4	**3d**	13.6
5	**3e**	7.9
Standard	**Acarbose**	4.7

Table 2 Results of butyrylcholinesterase activities analysis (IC_{50} values of Meldrum's acid derivatives (**3a**–**3e**) using acarbose as standard)

S. no.	Compound codes	IC_{50} (mg/mL)
1	**3a**	1.2
2	**3b**	19
3	**3c**	2.9
4	**3d**	6.3
5	**3e**	7.5
Standard	**Galantamine hydrobromide**	4.7

2.9 mg/mL, respectively) which is higher than the standard galantamine hydrobromide (IC_{50} = 4.7 mg/mL). Interestingly, compound **3a** was found to be a dual inhibitor of both these enzymes.

Molecular docking analysis

Through comparative docking analysis, we selected the best docked conformers with the lowest binding energy and characterized their detailed binding pattern (Fig. 2). The calculated binding energies obtained through stable docked conformations of inhibitors in complex with α-glucosidase and BuChE are shown in Table 3.

To monitor the binding behavior thoroughly, detailed analysis of adjacent amino acids lying at the active site was carried out. Trp82 residue of BuChE which participates in controlling the peripheral anionic activity was actively involved in inhibitor binding. Similarly, residues of the oxyanion hole (Gly116 and Gly117), catalytic triad (Ser198 and His438) and anionic site (Tyr332) were also participated in

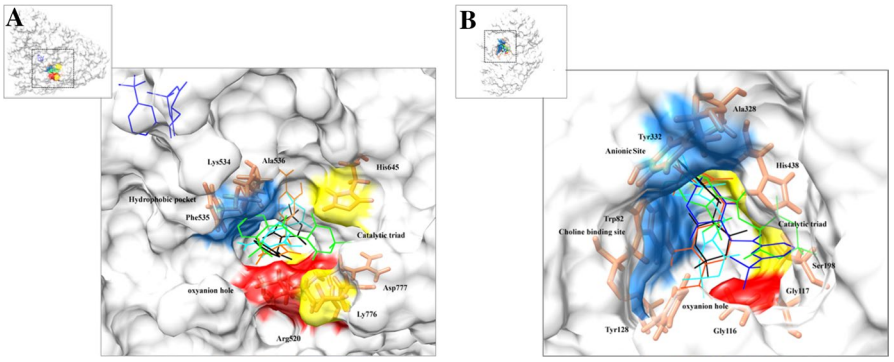

Fig. 2 Analysis of α-glucosidase and BuChE specific binding pockets. **a** α-Glucosidase pocket insight; **b** BuChE pocket insight. Labeled residues in stick representation indicate peripheral anionic site: Trp82 and Tyr332 (blue); catalytic triad: Ser198 and His438 (yellow); and oxyanion hole: GLY116 and GLY117 (red). Interacting residues of α-glucosidase and BuChE are depicted in coral color, while surface is shown in white color. The bound inhibitors are indicated by wire representation. Blue, inhibitor **3a**; orange, inhibitor **3b**; green, inhibitor **3c**; cyan, inhibitor **3d**; and black, inhibitor **3e**. (Color figure online)

Table 3 Energy scoring values and binding residues of α-glucosidase and BuChE with selected inhibitors

Compounds	α-Glucosidase		BuChE	
	Binding energy	Binding residues	Binding energy	Binding residues
3a	− 5.5	Val111, His113, Phe119, Ser120, Val166	− 6.79	Trp82, **Gly116**, **Gly117**, **Ser198**, Ala328, **His438**
3b	− 6.29	Pro284, Ala285, **Ser288,** Ala509, Arg520, Ser521, Phe522, **Ile523**, Gly533, Lys534, Phe535, Ala536, Ala537, Ile565, Pro566, Met567, Lys776	− 6.11	**Gly115**, Gly116, Glu197, Met437, Trp430, His438, Tyr332, Ala328, Phe329, Tyr440, **Trp82**, Leu125, Tyr128
3c	− 6.44	Glu114, Ala285, Leu286, Arg520, **Lys534**, Phe535, His645, Asp777	− 6.35	Trp82, Gly116, Gly117, Ser198, Ala328, His438, **Phe329**, Leu286, Phe398, Val288
3d	− 6.99	Ala285, Leu286, Pro287, Ala509, Arg520, Phe522, Ile523, Met567, Gly533, Lys534, Phe535, Ala536, Ala537, Lys776	− 7.49	Tyr332, Ala328, Phe329, Trp82, Tyr128, Gly115, Gly116, Gly439, His438, Gly78
3e	− 7.23	Ala285, Pro287, Leu286, Ala509, Arg520, **Ser521,** Phe522, Ile523, Lys534, Phe535, Ala536, Ala537, Met567, **Lys776**	− 6.81	Tyr332, Trp430, Ala328, Ser198, His438, Gly115, Gly116, Tyr128, Glu197, Gly439, Trp82

H-bonded residues are indicated in bold

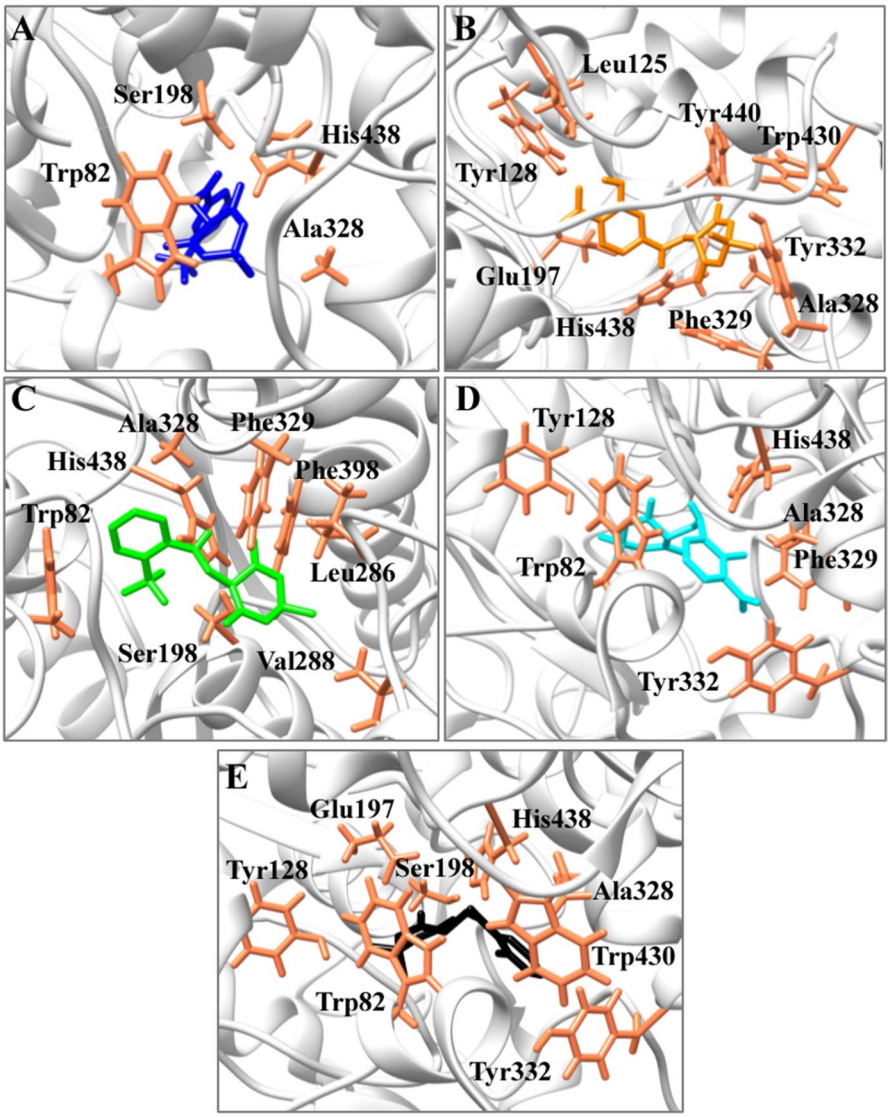

Fig. 3 Binding mode analysis. Best docked complexes of **(3a)** BuChE–inhibitor-1, **(3b)** BuChE–inhibitor-2, **(3c)** BuChE–inhibitor-3, **(3d)** BuChE–inhibitor-4 and **(3e)** BuChE–inhibitor-5. BuChE is shown in gray ribbon, while interacting residues are represented in coral sticks. Inhibitors are shown in stick representation

the inhibitor binding, thereby competing with substrate binding [32] (Figs. 2 and 3). Gly116, Gly117, Ser198, His438, Trp82 and Phe329 residues of BuChE were involved in hydrogen bonding. Despite these polar contacts, multiple hydrophobic interactions were also observed through Tyr128, Glu197, Val288, Ala328, Phe398 and Trp430 residues that appeared to assist in binding.

Furthermore, we evaluated the interactions of specified inhibitors with α-glucosidase. Majority of inhibitors exhibited binding at the Ala509–Asp777 region. It was observed that the residues of oxyanion hole, catalytic triad and hydrophobic pocket were actively engaged in interaction with the inhibitors (Figs. 2

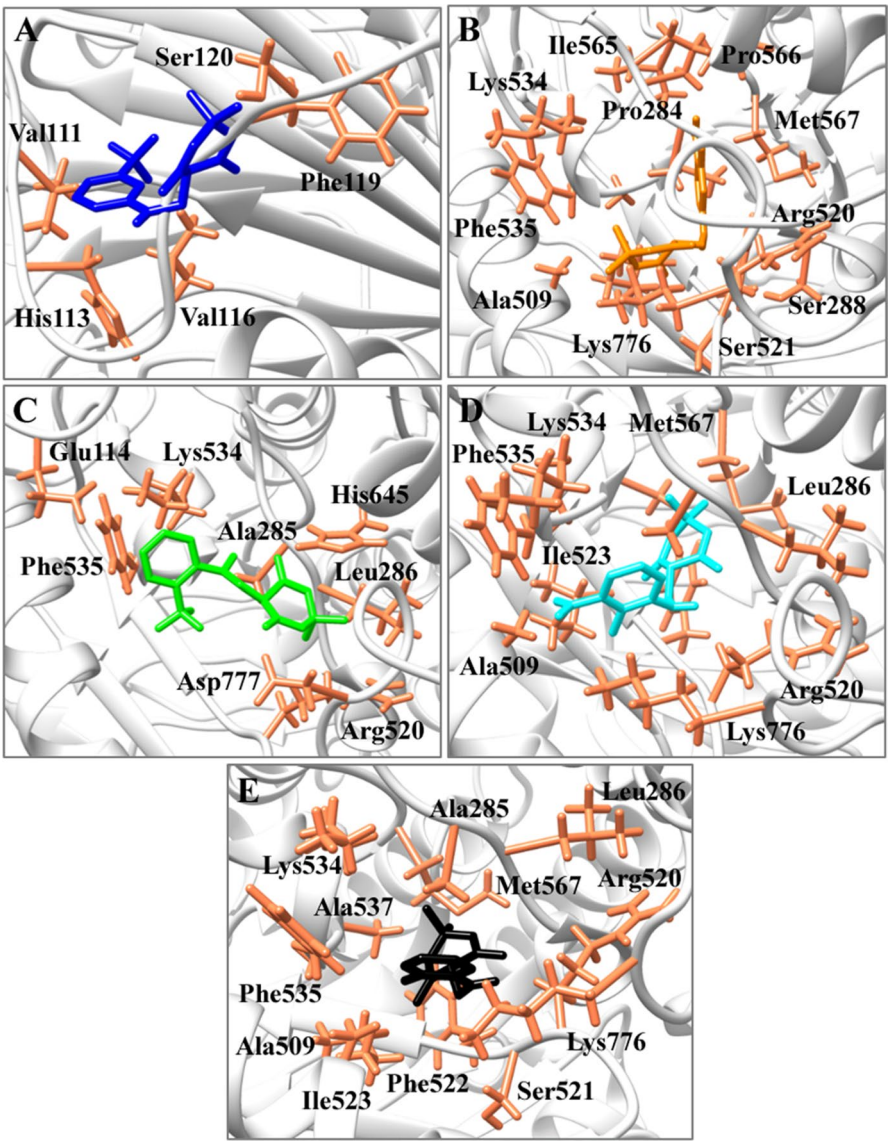

Fig. 4 Binding modes of inhibitor-bound α-glucosidase complexes. Best docked complexes of **(3a)** α-glucosidase–inhibitor-1, **(3b)** α-glucosidase–inhibitor-2, **(3c)** α-glucosidase–inhibitor-3, **(4d)** α-glucosidase–inhibitor-4 and **(4e)** α-glucosidase–inhibitor-5. α-Glucosidase is shown in gray ribbon, while interacting residues are represented in coral sticks. Inhibitors are shown in stick representation

and 4). Except inhibitor **3a**, others showed binding at similar binding cavity of α-glucosidase. Ala285, Ala509, Arg520, Ser521, Phe522, Ile523, Lys534, Phe535, Ala536, Ala537, Met567 and Lys776 residues of α-glucosidase were involved in binding. Overall, structural insights into inhibitor binding to the α-glucosidase and BuChE revealed significant contribution of hydrophobic regions and significant residues of active sites. LigPlots of BuChE–inhibitors complexes are investigated (Fig. 5), BuChE with inhibitors 1–5. BuChE residues that involved in H-bonding (green dotted lines) are shown in ball-and-stick representation, while brown semicircles represent hydrophobic residues of BuChE. All the results are comparable with experimental values.

Drug–DNA interaction studies

Concentration of DNA was determined by UV–visible spectrophotometer at 260 nm and was found 1.4×10^{-4} M. Spectroscopic titrations were done under normal body temperature (37 °C). The concentration of each synthesized compound (**3a**–**3e**) was prepared as 1.14×10^{-4} M. The absorbance measurements were taken by keeping the concentration of synthesized compounds (**3a**–**3e**) constant (1.4×10^{-4} M) in the sample cell, while varying the concentration of dsDNA in the sample cell. The change in absorbance was measured before and after the addition of various

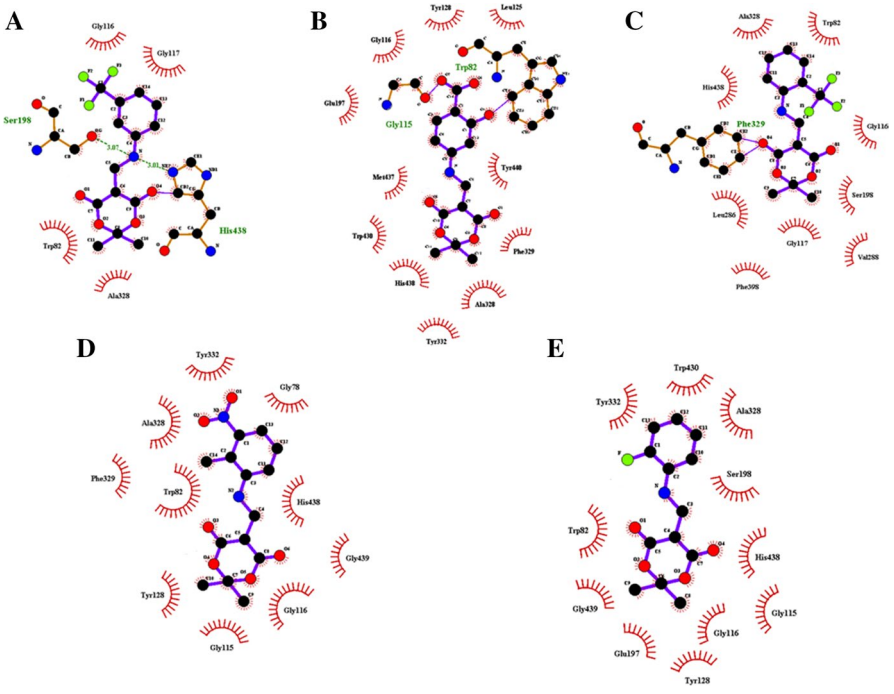

Fig. 5 LigPlots of BuChE–inhibitors complexes

concentrations of DNA. Solutions were allowed to stay for few minutes before each measurement so that equilibrium could be achieved between compound and DNA complex formation. Sample solutions were kept within the cell cavity for few seconds to assure the required temperature (37 °C).

The electronic absorption spectroscopy is one of the most useful techniques to study the drug–DNA interactions and provides a useful complement to other techniques used for DNA binding studies [33]. Commonly, hypochromic effect along with red or blueshift is observed in the absorption spectra of molecules if they intercalate with DNA.

UV spectra of five C-5-substituted Meldrum's acid were recorded separately by adding varying concentrations of DNA, and concentration effect of DNA on optimized concentration (1.4×10^{-4} M) of all the compounds was observed at body temperature (37 °C). The addition of DNA in aliquots was resulted in decrease in absorption peak intensity of the compounds with a slight blueshift of 1.0 nm, 1.2 nm, 0.1 nm and 0.4 nm, respectively, for compounds **3a**, **3b**, **3c**, **3d** and **3e**, respectively. A decrease in the peak intensities of **3a**, **3b**, **3c**, **3d** and **3e** in the presence of DNA was evaluated as 11.2%, 16.3%, 16.5%, 18.1% and 19.0%, respectively, using the following equation:

$$H\% = \frac{A_{\text{free}} - A_{\text{bound}}}{A_{\text{free}}} \times 100. \tag{1}$$

The observed hypochromic effect along with slight blueshift upon addition of DNA may correspond to the binding of compounds **3a**–**3e** with dsDNA through intercalative mode of interactions [34]. The decrease in peak intensity is related to decreased transition probabilities as coupling π-orbital is partially filled by electrons, which resulted in hypochromism in the spectra. On the other hand, a blueshift arises in the spectra due to improper coupling (conformational changes) of π^*-orbital of intercalated part of the compound with the π-orbital of the base pairs [34]. This distortion in the π-orbital of the base pairs and π^*-orbital of intercalated molecules resulted in unstacking of base pairs with hypochromic effect.

Determination of binding constants and free energy changes of compound–DNA complexes

Variation in absorbance of a compound in UV spectra in the presence of DNA leads to determine the binding constant "K_b" of compound–DNA complex using Benesi–Hildebrand equation [1, 33].

$$\frac{A_o}{A - A_o} = \frac{\varepsilon_G}{\varepsilon_{H-G} - \varepsilon_G} + \frac{\varepsilon_G}{\varepsilon_{H-G} - \varepsilon_G} \frac{1}{K_b[\text{DNA}]} \tag{2}$$

where K_b is the binding constant, A_o and A are the absorbance of the free and DNA-bound complex and ε_G and ε_{H-G} are their molar extinction coefficients, respectively. From the plot of $A_o/(A - A_o)$ against 1/[DNA], the ratio of the intercept to the slope furnished the value of binding constant, K_b (Fig. 6).

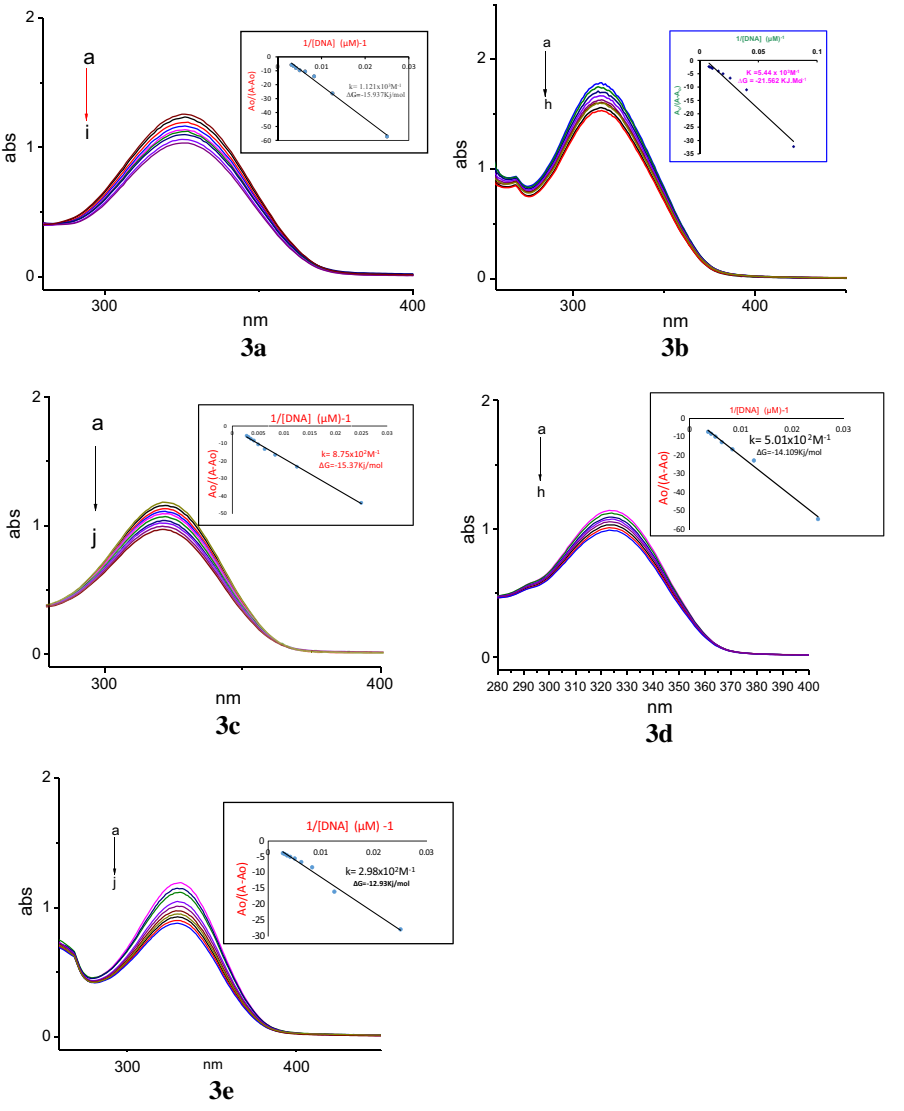

Fig. 6 DNA binding constant and Gibbs free energy calculations of synthesized compounds **3a**–**3e**. The arrow indicates the increasing concentration of DNA

The binding constant values (K_b) were evaluated for all the five compounds under physiological temperature (37 °C) and given in figures. K_b values for all compounds with DNA were found in the range of 10^2–0^3 M^{-1}. Binding constant values and UV spectral changes observed during ligand–DNA complex formation, i.e., hypochromic effect and hypochromic shift in the present study may further be credited to the small structure of molecules whose planer parts may possibility be intercalated between the adjacent DNA base pairs. Drug–DNA binding studies and Gibbs free

energy calculations were carried out using various concentrations of μM DNA such as 40, 80, 120, 160, 200, 240 and 280.

The inset graph represents the plot of $A_0/A - A_o$ versus 1/[DNA] $(\mu M)^{-1}$ for the calculation of the binding constant (k) and Gibbs free energy (ΔG). Since greater binding constant values are the measure of the complex stability, the values evaluated for all the synthesized compounds for their binding with DNA were found significant and may be inferred to the formation of stable compound–DNA complex [35–37]. Compound **3e** showed the comparatively greater K_b value (5.44×10^3 M^{-1}). The order of binding constants of Meldrum's acid derivatives (**3a**–**3e**) was found as follows:

$$K_b 3e > K_b 3c > K_b 3a > K_b 3b > K_b 3d.$$

Further, Gibbs free energies (ΔG) of novel Meldrum's acid DNA complexes were calculated by using the values of binding constant (K_b) in the following equation:

$$\Delta G = -RT \ln K_b.$$

Free energy changes were evaluated as negative values, indicating that all compounds **3a**–**3e** interacted spontaneously with DNA during compound–DNA complex formation. However, **3e** bound to the DNA more spontaneously as compared to other compounds as evident from its comparatively greater ΔG value. The order of complex spontaneity is not same as for binding constant: ΔG 3e > ΔG 3a > ΔG 3b > ΔG 3c > ΔG 3d.

Structure–activity relationship

As explained above, compounds with different substitutions on the aromatic ring linked with Meldrum's acid via olefinic bond were designed and synthesized **(3a–3e)**. Electron-withdrawing group, such as CF_3, enhanced inhibitory against both enzymes

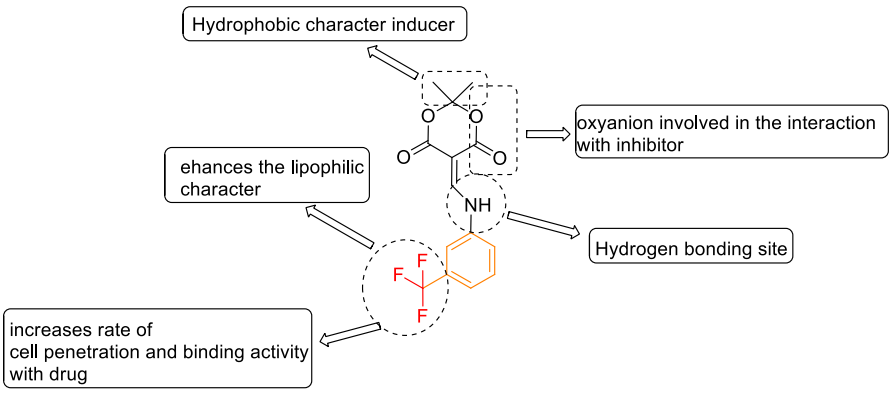

Fig. 7 Structure–activity relationship of the most potent and dual inhibitor of α-glucosidase and butyrylcholinesterase

(α-glucosidase and BChE). On the contrary, electron-donating groups, such as methyl and hydroxyl, decreased the enzyme inhibition activity (Fig. 7). The derivative in **3a** and **3c** bears CF_3 groups and in **3a** CF_3 group is at *meta* position and showed higher activity compared to **3c** against butyrylcholinesterase enzyme. However, NO_2 group was found to decrease the inhibitory activity. To be more precise, CF_3 group at *meta* position in compound **3a** exhibited excellent activity against both enzymes and found to be a dual inhibitor of both enzymes. The induction of fluorine atom in organic molecules enhances the lipophilic character which as a result increases the rate of cell penetration and transport of a drug to an active site [38, 39]. The higher polarizability due to the C–F bond may give new possibilities for binding to the receptor. Overall, the CF_3 groups at meta position are the main cause of excellent activity of **3a**.

Conclusions

A novel small set of compounds 2,2-dimethyl-5{[3(substituted-phenyl]amino} methylene)-1,3-dioxane-4,6-dione was designed and synthesized in excellent yield (73%-83%). The synthesized compounds **(3a–3e)** were subjected to enzyme inhibition activities (α-glucosidase and butyrylcholinesterase). The derivative **3a** showed higher activity compared to standards used (acarbose and galantamine hydrobromide) and was coincidently found to be most potent dual inhibitor of both enzymes. The derivatives **3a** and **3c** showed activity higher than the standard in butyrylcholinesterase enzyme inhibition, whereas compound **3a** showed excellent inhibition (IC_{50} value 2.1 which was found to be higher than the standard acarbose IC_{50} 4.7) against α-glucosidase. The other compounds showed moderate inhibition against these two enzymes. Comparative molecular docking studies were performed, and it was observed that the residues of oxyanion hole, catalytic triad and hydrophobic pocket were actively engaged in interaction with the inhibitor. The DNA–drug binding studies were performed to evaluate the interaction of compounds and calculate DNA binding constant and Gibbs free energy. DNA binding constant was found in the order K_b 3e > K_b 3c > K_b 3a > K_b 3*b* > K_b 3d, while Gibbs free energy was found in the order ΔG 3e > ΔG 3a > ΔG 3b > ΔG 3c > ΔG 3d. Density functional theory (DFT) calculations were done to investigate chemical insights (HOMO–LOMO) and charge density.

Acknowledgements Authors are thankful to Quaid-i-Azam University, Islamabad, Pakistan, for providing healthy research environment.

Compliance with ethical standards

Conflict of interest The authors declare no conflict of interest.

References

1. R. Raza, A. Saeed, M. Arif, S. Mahmood, M. Muddassar, A. Raza, J. Iqbal, Chem. Biol. Drug Des. **80**, 605 (2012)

2. A. Saeed, S. Zaib, S. Ashraf, J. Iftikhar, M. Muddassar, K.Y.J. Zhang, J. Iqbal, Bioorg. Chem. **63**, 58 (2015)
3. J. Iqbal, S. Zaib, A. Saeed, M. Muddassar, Lett. Drug Des. Discov. **12**, 488 (2015)
4. F.A. Larik, A. Saeed, M. Faisal, S. Hamdani, F. Jabeen, P.A. Channar, A. Mumtaz, I. Khan, M.A. Kazi, Q. Abbas, J. Mol. Struct. **1203**, 127459 (2020)
5. X. Zhang, K.P. Rakesh, S.N.A. Bukhari, M. Balakrishna, H.M. Manukumar, H.L. Qin, Bioorg. Chem. **80**, 86 (2018)
6. M. Wang, K.P. Rakesh, J. Leng, W.Y. Fang, L. Ravindar, D. Channe Gowda, H.L. Qin, Bioorg. Chem. **76**, 113 (2018)
7. W.Y. Fang, L. Ravindar, K.P. Rakesh, H.M. Manukumar, C.S. Shantharam, N.S. Alharbi, H.L. Qin, Eur. J. Med. Chem. **173**, 117 (2019)
8. C. Zhao, K.P. Rakesh, L. Ravidar, W.Y. Fang, H.L. Qin, Eur. J. Med. Chem. **162**, 679 (2019)
9. K.P. Rakesh, C.S. Shantharam, M.B. Sridhara, H.M. Manukumar, H.-L. Qin, Medchemcomm **8**, 2023 (2017)
10. J. Leng, H.L. Qin, K. Zhu, I. Jantan, M.A. Hussain, M. Sher, M.W. Amjad, M. Naeem-ul-Hassan, W. Ahmad, S.N.A. Bukhari, Chem. Biol. Drug Des. **88**, 889 (2016)
11. G.F. Zha, C.P. Zhang, H.L. Qin, I. Jantan, M. Sher, M.W. Amjad, M.A. Hussain, Z. Hussain, S.N.A. Bukhari, Bioorganic. Med. Chem. **24**, 2352 (2016)
12. M. Wang, H.L. Qin, J. Leng, M.W. Amjad, M.A.G. Raja, M.A. Hussain, S.N.A. Bukhari, Chem. Biol. Drug Des. **92**, 189 (2018)
13. X. Zhang, K.P. Rakesh, C.S. Shantharam, H.M. Manukumar, A.M. Asiri, H.M. Marwani, H.-L. Qin, Bioorg. Med. Chem. **26**, 340 (2018)
14. G.F. Zha, H.L. Qin, B.G.M. Youssif, M.W. Amjad, M.A.G. Raja, A.H. Abdelazeem, S.N.A. Bukhari, Eur. J. Med. Chem. **135**, 34 (2017)
15. A. Saeed, P.A. Mahesar, S. Zaib, M.S. Khan, A. Matin, M. Shahid, J. Iqbal, Eur. J. Med. Chem. **78**, 43 (2014)
16. J. Iqbal, A. Saeed, S.J.A. Shah, M. Al-Rashida, S. Mahmood, Med. Chem. (Los Angeles) **12**, 74 (2016)
17. S.J. Cano, H.B. Posner, M.L. Moline, S.W. Hurt, J. Swartz, T. Hsu, J.C. Hobart, J. Neurol. Neurosurg. Psychiatry **81**, 1363 (2010)
18. M. Faisal, F.A. Larik, M. Salman, A. Saeed, Kinet. Catal. **60**, 522 (2019)
19. M. Faisal, A. Haider, Q. Ul Aein, A. Saeed, F.A. Larik, Front. Chem. Sci. Eng. **13**, 586 (2019)
20. M.S. Malamas, J. Sredy, I. Gunawan, B. Mihan, D.R. Sawicki, L. Seestaller, D. Sullivan, B.R. Flam, J. Med. Chem. **43**, 995 (2000)
21. R. Maccari, R. Ottanà, C. Curinga, M.G. Vigorita, D. Rakowitz, T. Steindl, T. Langer, Bioorg. Med. Chem. **13**, 2809 (2005)
22. R. Maccari, P. Paoli, R. Ottanà, M. Jacomelli, R. Ciurleo, G. Manao, T. Steindl, T. Langer, M.G. Vigorita, G. Camici, Bioorg. Med. Chem. **15**, 5137 (2007)
23. Y. Ma, S. Sun, X. Cheng, S. Wang, W. Dong, R. Wang, W. Xu, Chem. Biol. Drug Des. **82**, 595 (2013)
24. S. Yamagishi, Curr. Diabetes Rev. **1**, 93 (2005)
25. A.R. Renslo, J.H. McKerrow, Nat. Chem. Biol. **2**, 701 (2006)
26. B.B. Mishra, R.R. Kale, R.K. Singh, V.K. Tiwari, Fitoterapia **80**, 81 (2009)
27. H.S. Sandhu, S. Sapra, M. Gupta, K. Nepali, R. Gautam, S. Yadav, R. Kumar, S.M. Jachak, M. Chugh, M.K. Gupta, Bioorg. Med. Chem. **18**, 5626 (2010)
28. G.M.M. Sampaio, A.M.R. Teixeira, H.D.M. Coutinho, D.M.S. Junior, P.T.C. Freire, R.R.F. Bento, L.E. Silva, EXCLI J. **13**, 1022 (2014)
29. M. Faisal, S. Hussain, A. Haider, A. Saeed, F.A. Larik, Chem. Pap. **73**, 1053 (2019)
30. M. Faisal, F.A. Larik, A. Saeed, J. Porous Mater. **26**, 455 (2019)
31. M. Faisal, M. Ahmed, S. Hussain, F.A. Larik, A. Saeed, Green Process. Synth. **8**, 635 (2019)
32. G.A. Kraus, P.K. Choudhury, Tetrahedron Lett. **42**, 6649 (2001)
33. M. Adib, E. Sheikhi, A. Kavoosi, H.R. Bijanzadeh, Tetrahedron **66**, 9263 (2010)
34. E. Fillion, D. Fishlock, Org. Lett. **5**, 4653 (2003)
35. M.J. Frisch, G.W. Trucks, H.B. Schlegel, G.E. Scuseria, M.A. Robb, J.R. Cheeseman, G. Scalmani, V. Barone, B. Mennucci, G.A. Petersson, H. Nakatsuji, Gaussian 09 Revision D. 01, vol. 93 (Gaussian Inc., Wallingford CT, 2009)
36. A.D. Becke, J. Chem. Phys. **98**, 5648 (1993)

37. F.A. Larik, M. Faisal, A. Saeed, P.A. Channar, J. Korabecny, F. Jabeen, I.A. Mahar, M.A. Kazi, Q. Abbas, G. Murtaza, Bioorg. Chem. **86**, 473 (2019)
38. M. Faisal, Z.U. Rehman, Q. Ul Aein, A. Saeed, Mater. Chem. Phys. **231**, 272 (2019)
39. F.A. Larik, A. Saeed, M. Faisal, P.A. Channar, S.S. Azam, H. Ismail, E. Dilshad, B. Mirza, Comput. Biol. Chem. **77**, 193 (2018)

Affiliations

Haroon Mehfooz[1] · Aamer Saeed[1] · Muhammad Faisal[1] · Fayaz Ali Larik[1] · Urooj Muqadar[1] · Saira Khatoon[1] · Pervaiz Ali Channar[1] · Hammad Ismail[3] · Salma Bilquees[1] · Sajid Rashid[4] · Shagufta Shafique[4] · Bushra Mirza[2] · Erum Dilshad[2] · Fawad Ahmad[1]

✉ Aamer Saeed
aamersaeed@yahoo.com

✉ Muhammad Faisal
mfaisal4646@gmail.com

✉ Fayaz Ali Larik
fayazali@chem.qau.edu.pk

[1] Department of Chemistry, Quaid-i-Azam University, Islamabad 45320, Pakistan

[2] Department of Biochemistry, Quaid-i-Azam University, Islamabad 45320, Pakistan

[3] Department of Biochemistry and Molecular Biology, University of Gujrat, Gujrat 50700, Pakistan

[4] National Centre for Bioinformatics, Quaid-I-Azam University, Islamabad 45320, Pakistan